American Journal of Botany 94(7): 1230–1247. 2007.

INFLORESCENCE DIVERSIFICATION IN THE "FINGER MILLET CLADE" (CHLORIDOIDEAE, POACEAE): A COMPARISON OF MOLECULAR PHYLOGENY AND DEVELOPMENTAL MORPHOLOGY[1]

QING LIU,[2,6] PAUL M. PETERSON,[3] J. TRAVIS COLUMBUS,[4] NANXIAN ZHAO,[2] GANG HAO,[5] AND DIANXIANG ZHANG[2]

[2]South China Botanical Garden, Chinese Academy of Sciences, Guangzhou, 510650, China;
[3]Department of Botany, National Museum of Natural History, Smithsonian Institution, Washington, D.C. 20013-7012 USA;
[4]Rancho Santa Ana Botanic Garden, 1500 North College Avenue, Claremont, California 91711-3157 USA; and
[5]College of Life Sciences, South China Agricultural University, Guangzhou, 510642, China

Within the Poaceae, inflorescence diversification and its bearing on phylogeny and evolution are exceedingly complex. We used phylogenetic information of the "finger millet clade," a group of grasses with digitate inflorescences, to study the inflorescence diversification. This clade appears monophyletic in the morphological and molecular phylogenetic analyses. Three well-supported clades are shown in our cpDNA-derived phylogeny, with clades I and III consisting of species of *Chloris* and *Microchloa*, respectively, and clade II including species of *Cynodon*, *Dactyloctenium*, and *Eleusine*. Variation appears at different times throughout development. Changes involving primordium number and arrangement occur very early, changes involving duration of primordium activity occur much later. Characters derived from the comparison of developmental sequences were optimized onto the most parsimonious tree. The developmental characters were congruent with the molecular phylogeny. Two developmental characters may not be homologous in the *Chloris* subclade and the *Cynodon* subclade.

Key words: Chloridoideae; development; finger millet clade; inflorescence; phylogeny; Poaceae.

Thirteen inflorescence forms found in the Chloridoideae (Poaceae) can be categorized into four basic inflorescence types: paniculate, digitate, racemose, and spicate (Liu et al., 2005a). These types can be characteristic of certain supra-generic groups, but analysis of the phylogenetic distribution of inflorescence types in their cladogram suggests that different forms have arisen independently many times (Liu et al., 2005b). Homoplasy of inflorescence types in the Chloridoideae phylogeny obscures the mechanism by which inflorescence diversification has arisen.

Mature inflorescences are seen only at a single stage of development, and this may not be sufficient to understand their morphological diversification and relationships (Doust and Kellogg, 2002; Stuessy, 2003). Therefore, it may be preferable to look for homologies during the development of an inflorescence rather than in the mature form.

We have chosen to concentrate on the so-called finger millet clade (subtribe Chloridineae), which has 17 genera and approximately 150 species, sensu clade C_1 in Hilu and Alice (2001). The finger millet clade has been found to be monophyletic in morphological (Van den Borre and Watson, 1997; Liu et al., 2005b) and molecular (Hilu and Alice, 2001) studies. It includes genera whose inflorescences appear digitate. Homology of inflorescence structures was not recognized by previous workers, who placed members of the clade in different tribes (Clayton and Renvoize, 1986). *Chloris*, *Cynodon*, *Dactyloctenium*, *Eleusine*, and *Microchloa* are the larger genera within the finger millet clade. By investigating these genera, we hope to discern developmental changes that have lead to the diversity seen in mature inflorescences (Figs. 1–6).

The study of inflorescence development among members in the finger millet clade may also improve our understanding of the nature of digitate branching. The branching system of the inflorescence has been viewed as a single, long paraclade or main axis (Vegetti, 1986), or as several long paraclades circling a truncated main axis (Cámara-Hernández and Rua, 1991; Liu et al., 2005a). Observing inflorescence development will allow many questions to be properly formulated.

To define developmental homologies and to evaluate evolutionary diversification, we must trace developmental characters based on an explicit phylogenetic hypothesis. Accurate assessments of developmental and phylogenetic homology will impact estimates of the inflorescence diversification as well as our perception of the evolutionary processes through which they have arisen (Hufford, 2003; Kellogg, 2004). The present study aims to (1) explore the precise developmental sequences and clarify the nature of the digitate branching system, and (2) assess the homology of developmental characters in the finger millet clade through integration of molecular phylogenetic and developmental analyses.

MATERIALS AND METHODS

Taxon sampling and sequencing—Nine ingroup and two outgroup taxa were sampled for the phylogenetic reconstruction (Appendix 1). The outgroup

[1] Manuscript received 25 May 2006; revision accepted 25 May 2007.

The authors thank Z.-R. Song and S.-F. Zhang for help with field collection; X.-L. Wang, J.-Y. Yao, and S.-L. Zhou for assistance in the molecular laboratory; X.-Y. Hu and Z.-W. Guo for their kind help with the SEM operation; and E. A. Kellogg, A. N. Doust, and G. H. Rua for valuable comments. This study was financially supported by the Smithsonian Institution Short-Term Visitor Awards to Q.L., South China Botanical Garden Director's Fund to Q.L. (2005–1140), Project of Bureau of Life Sciences and Biotechnology (2002–1091) of the Chinese Academy of Sciences to N.X.Z. (2002–1091), and partly supported by Operation Fund of Molecular Systematics Laboratory of SCBG (0790003002). The authors also thank two anonymous reviewers for their constructive comments that greatly improved the manuscript.

[6] Author for correspondence (e-mail: liuqing@scib.ac.cn)

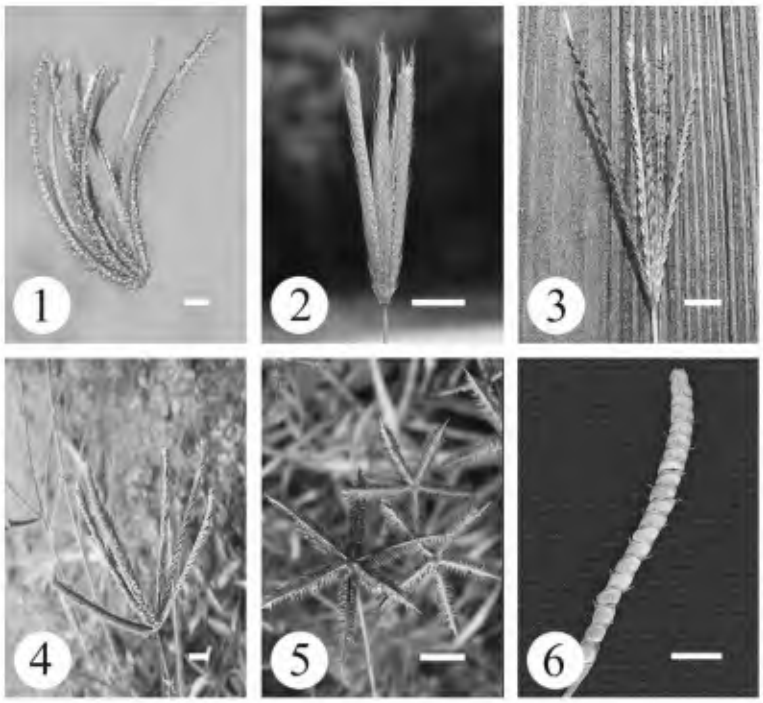

Figs. 1–6. Mature inflorescences. **1.** *Chloris barbata*. **2.** *C. virgata*. **3.** *Cynodon dactylon*. **4.** *Eleusine indica*. **5.** *Dactyloctenium aegyptium*. **6.** *Microchloa indica*. Scale bar = 10 cm.

taxa were chosen from the $x = 10$ *Eragrostis* clade (Hilu and Alice, 2001; Roodt and Spies, 2003). Ingroup taxa were chosen to show all of the different inflorescence forms in the finger millet clade. All samples were freshly collected in the field and were identified using keys in Keng (1959) and Chen (1990).

DNA was extracted with CTAB described in Doyle and Doyle (1987). Two chloroplast markers including *trnL* intron and *rps16* intron were selected because they are highly informative noncoding regions (Shaw and Small, 2004). These cpDNA regions were amplified using primers of Taberlet et al. (1991) for the *trnL* intron and of Oxelman et al. (1997) for the *rps16* intron. DNA amplifications were performed in 50 μL reactions with approximately 10–50 ng of total DNA, 10 mmol Tris buffer/L (100 mmol Tris-HCl/L pH 8.8, 250 mmol KCl/L), 0.2 μmol dNTPs/L, 10 μmol of each primer/L, 5 U of *Taq* polymerase, and 25 μmol $MgCl_2$/L. The polymerase chain reactions (PCR) was run on a Peltier Thermal Cycler DNA engine DYAD (MJ Research, Watertown, Massachusetts, USA) starting at 94°C for 3 min; followed by 33 cycles of 94°C for 1 min, 52°C for 1 min, and 72°C for 1 min; and ending with a final extension of 72°C for 7 min. To be cleaned for sequencing, the PCR products were then run on a 1% low-melting agarose gel, and the bands excised and gelased, using the GELase (Epicentre Technologies, Madison, Wisconsin, USA) method. Dideoxy cycle sequencing was conducted using BigDye version 3 reagents (Applied Biosystems, Foster City, California, USA) with an ABI model 377 automated sequencer (Applied Biosystems). Cycling conditions included an initial denaturing step at 94°C for 5 min, followed by 30 cycles of 96°C for 10 s, 50°C for 5 s, and 60°C for 4 min. Contigs were assembled using Sequencher 3.1.1 (Gene Codes, Ann Arbor, Michigan, USA). Sequences (Appendix 1) have been deposited in GenBank. They were then aligned by ClustalX version 1.83.1 (PC version) (Thompson et al., 1997) and manually adjusted using the program MacClade 4.0 (Maddsion and Maddsion, 2000).

Phylogenetic analyses—Phylogenetic analyses were performed with PAUP* 4.0b10 (Swofford, 2002) using maximum parsimony (MP) (Farris et al., 1970; Fitch, 1971) and maximum likelihood (ML) (Felsenstein, 1981) methods. The heuristic searches for MP analysis were conducted with 100 random taxon addition replicates, tree-bisection-reconnection (TBR) branch swapping, and collapse of zero-length branches. Character state changes were equally weighted in the analysis. Gaps were treated either as missing data or as new characters. The support values of clades revealed in the maximum parsimony tree(s) (MPTs) were examined using 1000 bootstrap replicates with the heuristic search options. Chi-square tests of PAUP* were run to reveal nucleotide bias among taxa. Congruence between the two chloroplast data sets was assessed with the incongruence length difference (ILD) test (Farris et al., 1995). The ILD test has been criticized as a method for assessing character incongruence (Yoder et al., 2001; Barker and Lutzoni, 2002). However, Hipp et al. (2004) has recently shown that the ILD test can serve as a conservative initial test of data partition congruence. The appropriate model for DNA substitution for the maximum likelihood analysis was determined using Modeltest version 3.06 (Posada and Crandall, 1998). Once the best-fit model was determined, maximum likelihood searches were performed on the data set (Felsenstein, 1981).

The best-fit analysis of the combined cpDNA data sets including *trnL* intron and *rps16* intron (including gap characters) was performed with WinClada version 1.00.08 (Nixon, 2002) running the program NONA (Goloboff, 1993) as a daughter process. In the NONA analysis, three sequential parsimony ratchet runs were chosen, and each replicate included 200 iterations with 20 trees held in memory. Support for cladistic relationships was assessed using bootstrap analysis (Felsenstein, 1985) with 1000 replications that included 10 searches and 10 starting trees in each replication.

Developmental analysis—Approximately 40 inflorescences in various developmental stages for all taxa (Appendix 1) were collected and preserved in FAA (1 part formalin, 1 part glacial acetic acid, 18 parts 70% ethanol). After dissection with a Nikon SM-Z645 stereomicroscope (Nikon, Tokyo, Japan), the samples were fixed overnight in 2% (v/v) glutaraldehyde in phosphate buffer at 4°C. The samples were then rinsed three times for 5 min each, and then kept 2 h in 1% osmium tetroxide (OsO_4, pH = 6.8) at room temperature. Samples were dehydrated in a series of ethanol solutions (70%, 90%, and 100% three times), critical point dried in an Eiko DX-1 critical-point dryer (Eiko Engineering, Hitachi, Japan), and sputter-coated with gold in a JFC-1100 sputter coater (JEOL, Tokyo, Japan). Inflorescences were examined and photographed with a Jeol JSM-6360V scanning electron microscope (SEM) (JEOL, Tokyo, Japan) at 10 kv. Use of continuous quantitative characters in phylogenetic analysis has been criticized by some authors (e.g., Stevens, 1991) but defended by others based on simulation studies and other empirical evidence (Poe and Wiens, 2000). Because of the lack of consensus on this topic and because our aim was

TABLE 1. Main characters of inflorescence development of the finger clade (coding for phylogenetic analysis is in brackets).

Character	*Chloris barbata* (clade I)	*Chloris virgata* (clade I)	*Cynodon dactylon* + *C. arcuatus* (clade II)	*Eleusine indica* + *E. coracana* (clade II)	*Dactyloctenium aegyptium* (clade II)	*Microchloa indica* + *M. kunthii* (clade III)	*Eragrostis pilosa* (outgroup)
Inflorescence							
1. Dp of 1°-axis primordium (μm)	44 [1]	57 [1]	44 [1]	39 [1]	26 [1]	23 [1]	126 [0]
2. Dt of 1°-axis primordium (μm)	56 [0]	76 [0]	55 [0]	26 [1]	24 [1]	17 [1]	83 [0]
3. 100·Dp/Dt of 1°-axis primordium	79 [1]	75 [1]	79 [1]	148 [0]	110 [0]	134 [0]	151 [0]
4. Shape of 1°-axis primordium	Suboblate [1]	Suboblate [1]	Suboblate [1]	Peroblate [0]	Peroblate [0]	Peroblate [0]	Peroblate [0]
5. Length of 1° axis at the moment of initiation of 2°-axis primordia (μm)	81 [1]	94 [1]	82 [1]	92 [1]	55 [1]	57 [1]	157 [0]
6. Number of 2°-axis primordia	3–9 [1]	5–7 [1]	3–6 [1]	2–7[1]	2–6 [1]	1 [1]	6–8 [0]
7. Arrangement of 2°-axis primordia	Verticillate [1]	Verticillate [1]	Verticillate [1]	Semiverticillate [1]	Semiverticillate [1]	Unilateral [2]	Alternative [0]
8. Angle between 1° axis and 2° axes	25° [1]	12° [1]	40° [1]	55° [0]	85° [0]	18° [1]	65° [0]
9. Length of 2° axis at the moment of initiation of 3°-axis primordia (μm)	630 [1]	432 [2]	325 [2]	646 [1]	666 [1]	320 [2]	790 [0]
10. End of 2° axis	A blind extension [1]	A blind extension [1]	A spikelet	A spikelet [0]	A microtip [2]	A microtip [2]	A spikelet [0]
11. Peduncle length (mm)	1.5 [0]	2.5 [0]	[0]	3.1 [0]	9.0 [1]	2.6 [0]	2.8 [0]
Spikelet							
12. Dp of proximal spikelet primordium (μm)	23 [0]	22 [0]	45 [1]	30 [0]	30 [0]	9 [0]	36 [0]
13. Dp of distal spikelet primordium (μm)	51 [1]	72 [0]	33 [1]	36 [1]	29 [1]	13 [1]	30 [0]
14. 100·Dp/Dt of spikelet primordia	84 [0]	84 [0]	57 [1]	35 [1]	36 [1]	35 [1]	88 [0]
15. Shape of spikelet primordia	Suboblate [0]	Suboblate [0]	Oblate [1]	Peroblate [2]	Peroblate [2]	Peroblate [2]	Suboblate [0]
16. Initiation succession of spikelets on 2° axis	Basipetal [1]	Basipetal [1]	Amphipetal [2]	Basipetal [1]	Amphipetal [2]	Basipetal [1]	Acropetal [0]
17. Compression of spikelets	Lateral [0]	Lateral [0]	Lateral [0]	Lateral [0]	Lateral [0]	Dorsal [1]	Lateral [0]
18. End of spikelet axis	Lemma [0]	Lemma [0]	A perfect floret [1]	Lemma and palea [0]	A perfect floret [1]	An imperfect floret [1]	Lemma and palea [0]
Floret							
19. Floret number per spikelet	4 [1]	2 [1]	2 [1]	5 [1]	3 [1]	1 [2]	6 [0]
20. Maturation of florets per spikelet	Some [0]	Some [0]	All [1]	Some [0]	All [1]	All [1]	Some [0]
21. Dt of stamen primordium (μm)	18 [1]	18 [1]	14 [1]	18 [1]	13 [1]	20 [1]	23 [0]
22. Dt of gynoecial primordium (μm)	16 [1]	16 [1]	16 [1]	15 [1]	19 [1]	19 [1]	23 [0]
23. Dt of theca (μm)	57 [1]	58 [1]	42 [1]	45 [1]	36 [1]	43 [1]	129 [0]

Note: Dp = polar (longitudinal) axis diameter; Dt = equatorial (transverse) axis diameter.

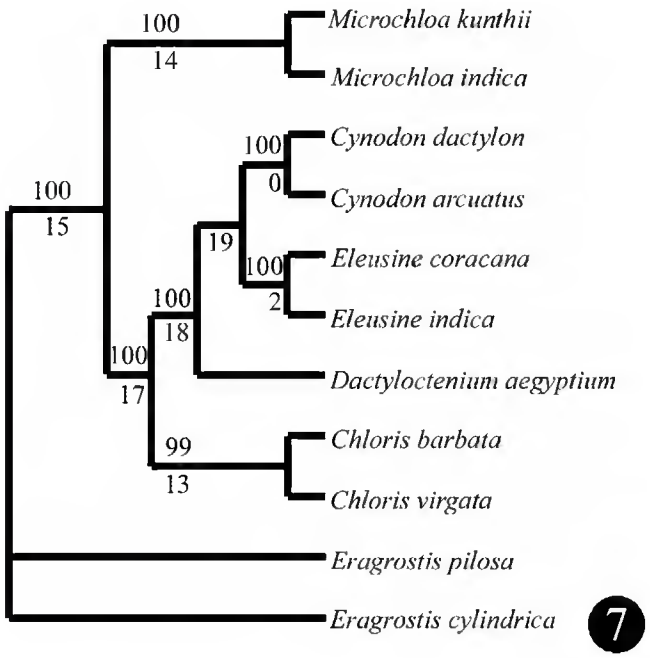

Fig. 7. Single parsimonious tree of the combined analysis of *trnL* intron and *rps16* intron data sets. Tree length = 989, consistency index (CI) = 0.94, retention index (RI) = 0.97. Numbers above branches are bootstrap values.

to define the homology of continuous quantitative characters, we decided to include continuous quantitative characters in our analyses.

Polar (longitudinal) axis diameter (Dp) and equatorial (transverse) axis diameter (Dt) of primordium were calculated using SEM photos, and interpretation of Dp/Dt corresponding to different primordium shapes follows Erdtman (1952). Twenty-three characters were selected on the basis of intergeneric variations (Table 1). They consisted of 17 binary and six multistate characters. All multistate characters were treated as unordered. Six quantitative characters were coded following the step matrix gap weighting (SMGW) method of Wiens (2001). The SMGW method assigned to each quantitative character a unique mean value, and the changes between these states are specified in a step matrix (Appendix S1 in Supplemental Data accompanying the online version of this article).

Mapping characters—WinClada (Nixon, 2002) was used to optimize (Fitch, 1971) inflorescence characters on the most parsimonious tree inferred from the combined molecular data set.

RESULTS

Phylogeny analysis—Chi-square tests of homogeneity of base frequencies across taxa were run in PAUP* for the nonambiguous sites for (1) all 11-taxon *trnL* intron data ($\chi^2 = 4.7645$, df = 30, $P = 1$), *rps16* intron data ($\chi^2 = 12.3213$, df = 30, $P = 0.99$), or combined *trnL* intron and *rps16* intron data ($\chi^2 = 38.0047$, df = 30, $P = 0.15$), and for (2) ingroup 9-taxon concatenated *trnL* intron and *rps16* intron, using the nonambiguous sites ($\chi^2 = 27.6696$, df = 24, $P = 0.27$). None of the tests revealed nucleotide bias among taxa. The *trnL* intron alignment comprised 591 positions, of which 315 were parsimony informative characters. The *rps16* intron alignment comprised 853 positions, of which 451 were parsimony informative characters. Because these two cpDNA data sets were found to be congruent using the ILD test ($P = 1.00$), we combined them. The combined data set of 11 taxa comprised 1444 positions, 766 of which were parsimony informative.

With gaps scored as missing data, the MP analysis of the combined data set generated one MPT with a total length of 990 steps, a consistency index (CI) excluding uninformative characters of 0.96, a retention index (RI) of 0.98, and a rescaled consistency index (RC) of 0.94 (Fig. 7). *Microchloa*, *Cynodon*, *Eleusine*, *Dactyloctenium*, and *Chloris* formed a monophyletic group in one most parsimonious tree. Within this finger millet clade, three major clades were recovered, with clades I and III consisting of species of *Chloris* and *Microchloa*, respectively, clade II including species of *Cynodon*, *Eleusine*, and *Dactyloctenium*. Bootstrap support for clades I, II, and III was 99%, 100%, and 99%, respectively. Clade III is revealed to be sister to the clades I and II. Even when the gaps were treated as new characters, the topology of the tree did not change. Modeltest suggested that the GTR + I + G was the best model (−ln likehood score = 5392.73). The base frequencies were A = 0.33, C = 0.17, G = 0.16, T = 0.35, and the substitution rate matrix was as follows: A/C = 0.14, A/G = 0.25, A/T = 0.10, C/G = 0.14, C/T = 0.22, G/T = 0.15, the Ti/Tv = 0.81. The gamma shape parameter was 1.85. The maximum likelihood tree (not shown) had an almost identical topology to the MPT (Fig. 7) except that *Chloris barbata* and clade II formed a monophyletic group, sister to *C. virgata*. Owing to the lack of resolution of monophylesis for *Chloris* in the ML analysis, the MP tree was chosen to map the developmental characters on our cladogram.

Development—Early inflorescence development in all species of the finger millet clade is similar. The beginning of inflorescence development can be identified by the elongation of the shoot apex meristem as it undergoes the transition from vegetative to reproductive growth (Figs. 8, 28, 46, 64, 82). Other aspects of development vary widely, and therefore the development of different genera will be discussed separately. For the purposes of discussion, we here define the main inflorescence axis as the first (1°) axis, the major branches as secondary (2°) axes, the branches on the major branches as tertiary (3°) axes, and so on.

Chloris—Inflorescence development of *Chloris* starts with the formation of a suboblate 1°-axis primordium (Fig. 8). Elongation of the 1° axis stops (Fig. 9) after initiation of three to nine 2°-axis primordia in *C. barbata* (Fig. 10) and five to seven 2°-axis primordia in *C. virgata*. These 2°-axis primordia are verticillate and surround the arrested 1° axis (Fig. 11). When these 2°-axis primordia elongate to nearly 432–630 μm, the suboblate 3°-axis (i.e., spikelet) primordia initiate basipetally on the 2° axis (Fig. 12). In *C. barbata*, the proximal spikelet primordium (Fig. 13) is 50% smaller than the distal one (Fig. 14), while in *C. virgata*, the proximal spikelet primordium is less than one third the size of that of the upper one (Table 1). In both species, the spikelet primordia are distichous along the abaxial surface of the 2° axis.

Spikelet differentiation on the 2° axis of *Chloris* is basipetal (Fig. 15) and starts with the inception of two alternate concave glume primordia. The first formed primordium develops into a lower glume and the second one into an upper glume (Fig. 16). The glume arrangement along the 2° axis is similar in all examined species where the lower glume of spikelet is central, in contrast to lateral upper glume of spikelets on the abaxial surface of the 2° axis. In *C. barbata*, four lemma primordia on

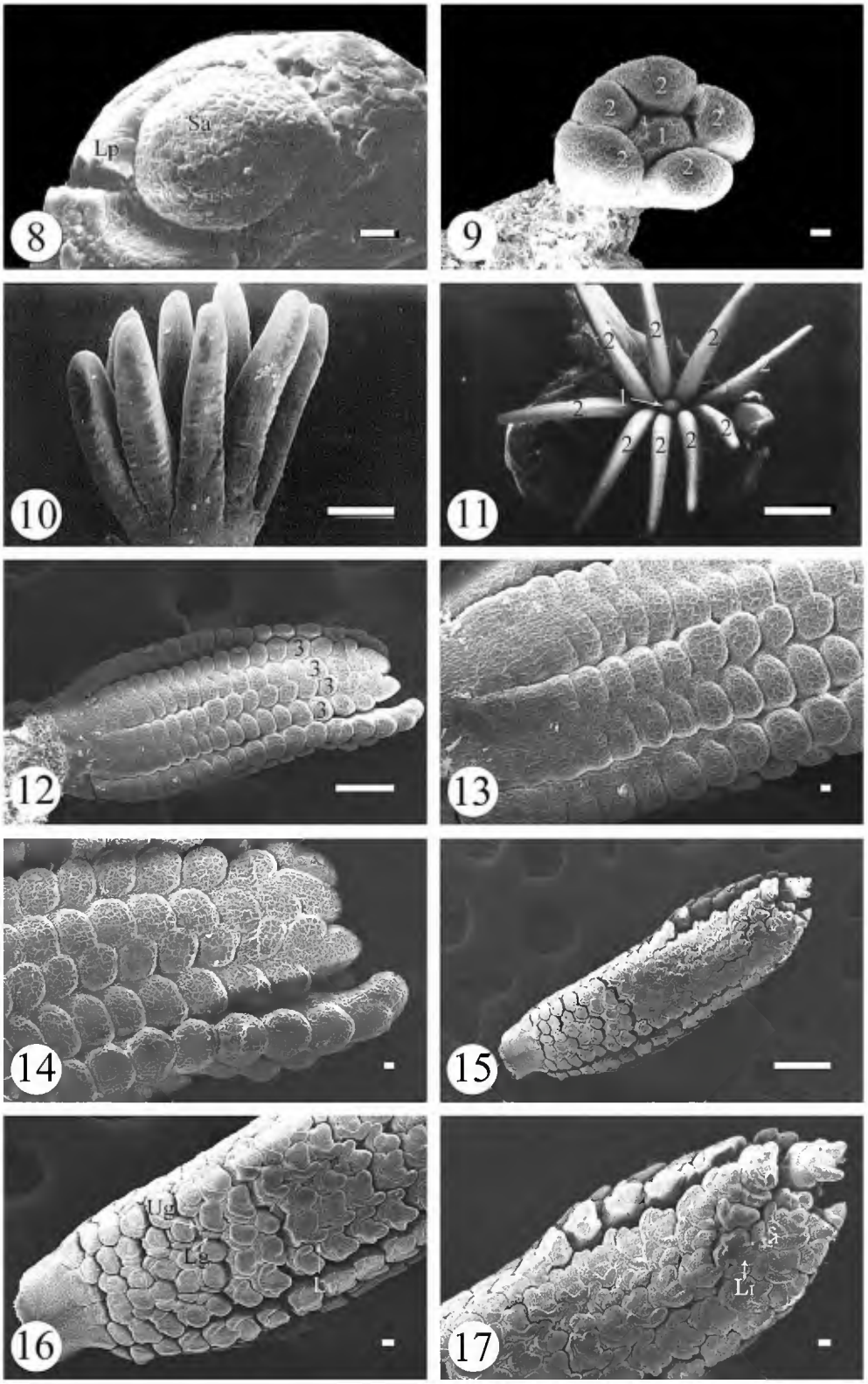

Figs. 8–17. *Chloris barbata* SEM micrographs. **8.** Vegetative shoot apex. **9.** Elongation of the 1°-axis primordium and initiation of 2°-axis primordia. **10.** Elongation of 2° primordia. **11.** Polar view of verticillate arrangement of 2° axes surrounding the arrested 1° axis. **12.** Initiation of suboblate 3°-axis primordia in basipetal succession. **13.** Proximal spikelet primordia of the 2° axis. **14.** Distal spikelet primordia of the 2° axis. **15.** Differentiation of spikelet primordia in basipetal succession. **16.** Initiation of glumes and the first lemma. **17.** Initiation of first floret primordium. Scale bars = 10 μm in Figs. 8, 9, 13, 14, 16, 17; 100 μm in Figs. 10–12, 15. *Figure abbreviations*: 1, 1° axis; 2, 2° axis; 3, 3° axis; A, anther; f1, first floret; f2, second floret; f3, third floret; f4, fourth floret; f5, fifth floret; G1, gynoecium of f1; Gr, gynoecial ridge; L1, lemma of f1; L2, lemma of f2; L3, lemma of f3; L4, lemma of f4; L5, lemma of f5; Lg, lower glume; Lo, lodicule; Lp, leaf primordium; Ov, ovule; P1, palea of f1; S, spikelet primordium; Sa, shoot apex; St, stamen; Ug, upper glume.

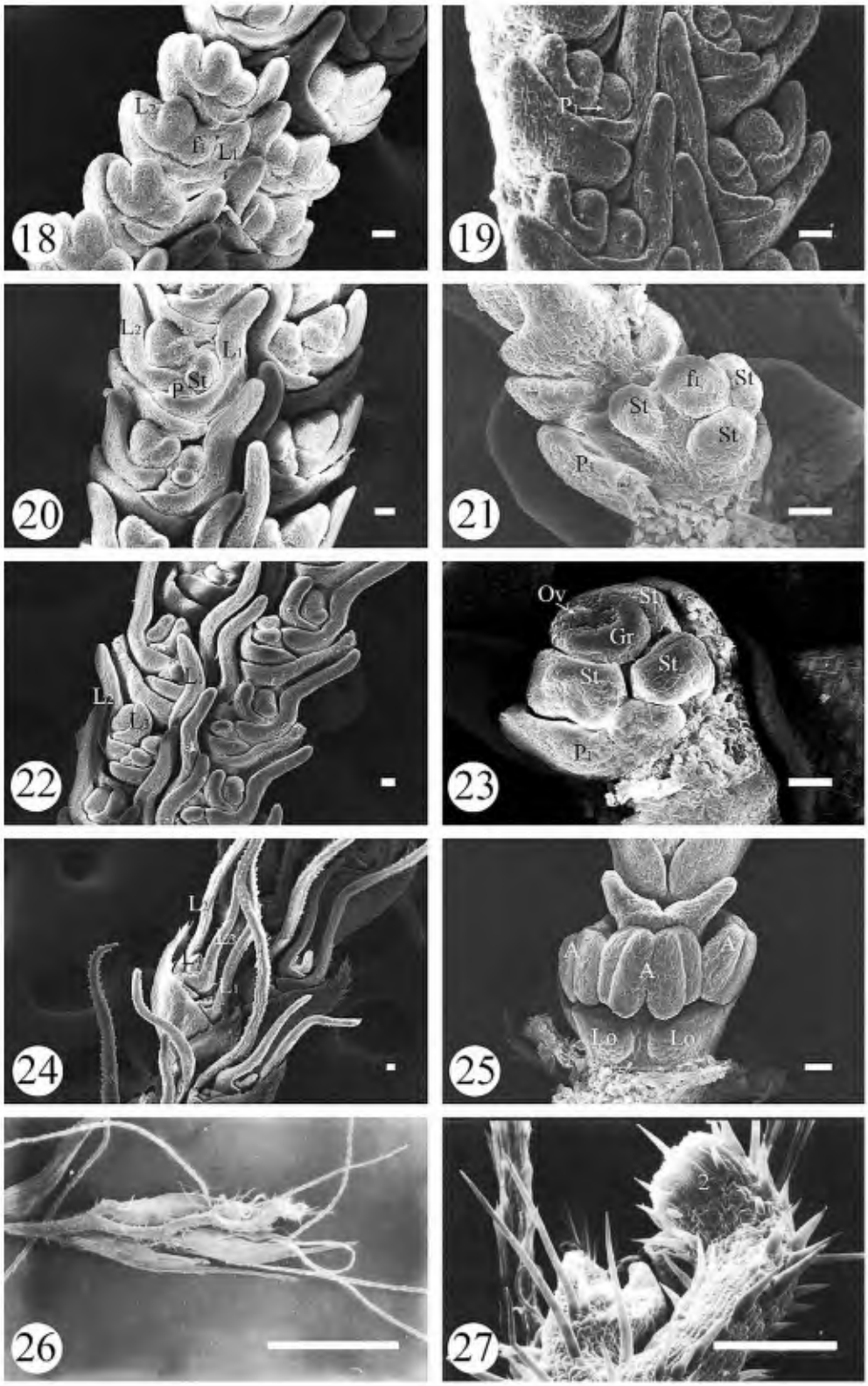

Figs. 18–27. *Chloris barbata* and *C. virgata* SEM micrographs. Figs. 18–25. *C. barbata*. **18.** Initiation of second lemma. **19.** Initiation of palea of first floret. **20.** Elongation of lemmas and differentiation of floral organs of first floret. **21.** The first floret of left spikelet in Fig. 20, initiation of stamen. **22.** Initiation of third lemma and differentiation of gynoecium of first floret. **23.** The first floret of left spikelet in Fig. 22, initiation of gynoecial ridge. **24.** Initiation of fourth lemma and differentiation of anther of first floret. **25.** The first floret of left spikelet in Fig. 24, initiation of lodicules and anther. Figs. 26–27. *C. virgata*. **26.** Two protruding awns of every spikelet in *C. virgata*. **27.** A blind extension in the 2°-axis apex. Scale bars = 10 μm in Figs. 18–25; 100 μm in Figs. 26–27. See Figs. 8–17 for abbreviations.

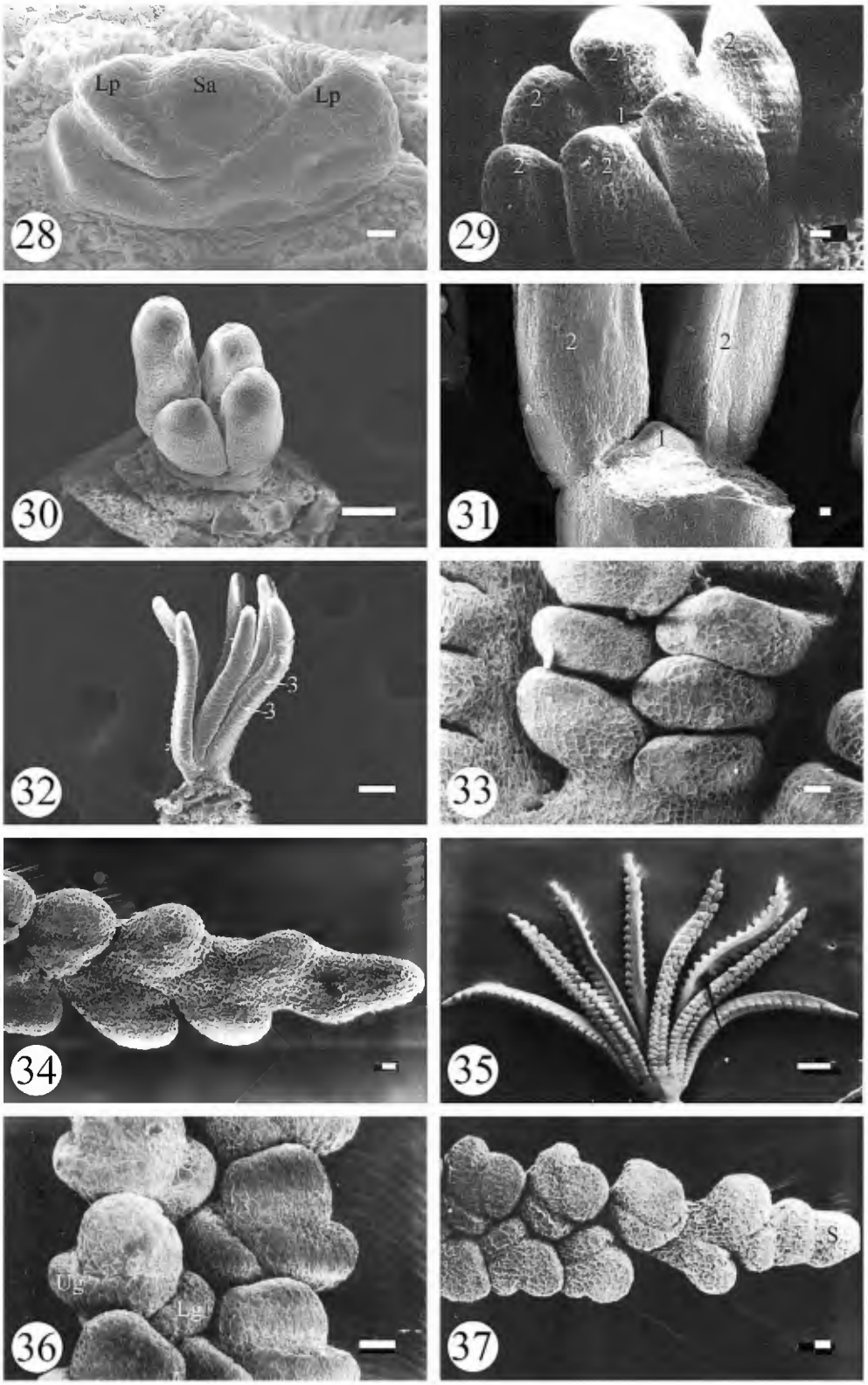

Figs. 28–37. *Cynodon dactylon* SEM micrographs. **28.** Vegetative shoot apex. **29.** Elongation of the 1°-axis primordium and initiation of 2°-axis primordia. **30.** Elongation of 2°-axis primordia. **31.** Verticillate arrangement of 2°-axis primordia surrounding the arrested 1° axis, front two 2°-axis primordia removed. **32.** Initiation of oblate 3°-axis primordia in amphipetal succession. **33.** Proximal spikelet primordia of the 2° axis. **34.** Distal spikelet primordia of the 2° axis. **35.** Differentiation of spikelet primordia in amphipetal succession. **36.** Initiation of lower and upper glumes. **37.** An indifferent spikelet primordium in 2°-axis apex. Scale bars = 10 μm in Figs. 28, 29, 31, 33–37; 100 μm in Figs. 30, 32. See Figs. 8–17 for abbreviations.

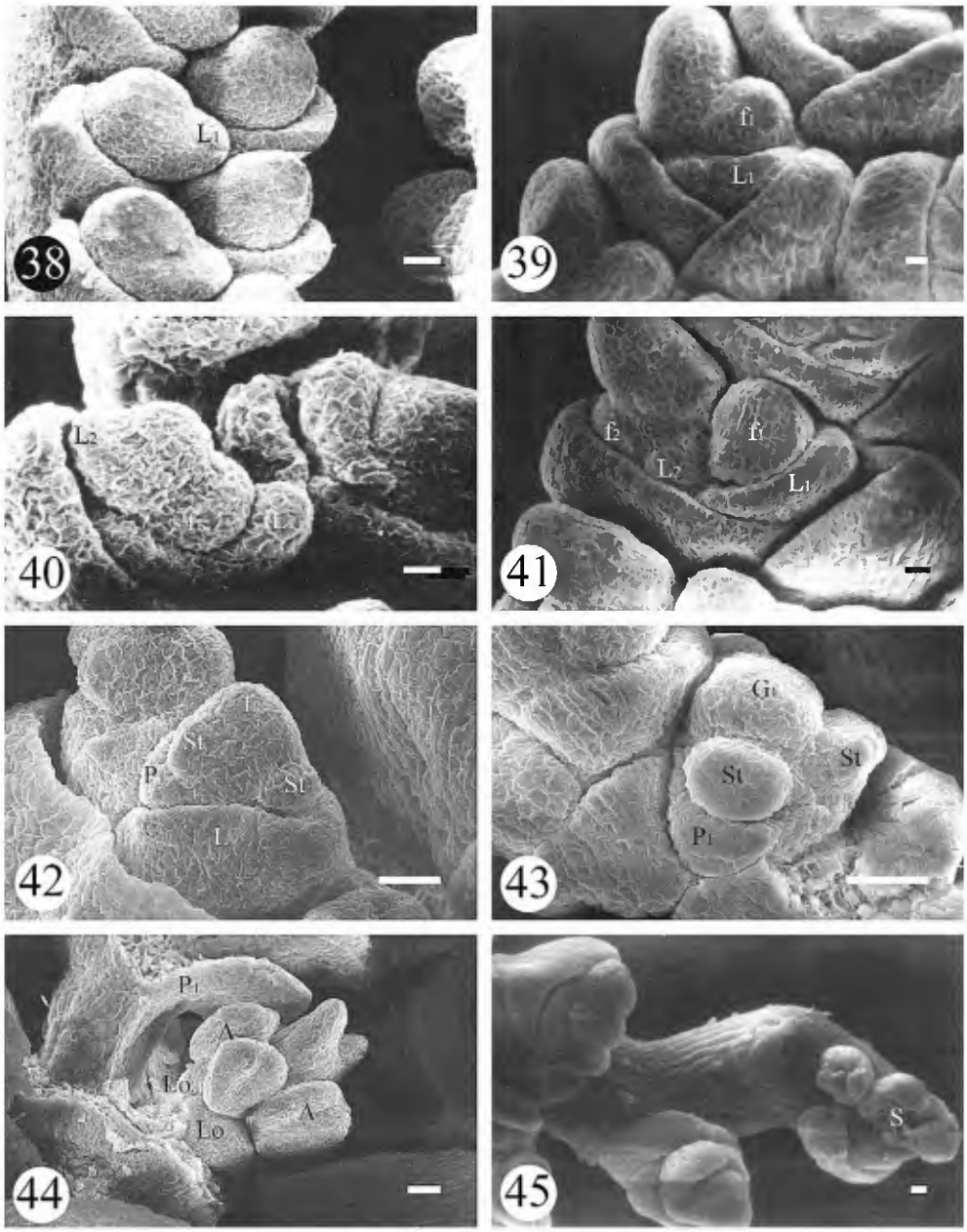

Figs. 38–45. *Cynodon dactylon* SEM micrographs. **38.** Initiation of first lemma. **39.** Initiation of first floret primordium. **40.** Initiation of second lemma. **41.** Initiation of second floret primordium. **42.** Initiation of palea and stamen of first floret. **43.** Initiation of gynoecium of first floret. **44.** Differentiation of lodicules and anther of first floret. **45.** A degenerative spiketet in 2°-axis apex. Scale bar = 10 μm. See Figs. 8–17 for abbreviations.

each spikelet are initiated in turn, while in *C. virgata* only two lemma primordia are initiated. The first floret of every spikelet differentiates and matures first (Figs. 20, 22, 24), while the remainder of the floret primordia are undifferentiated. When the spikelet axis elongates in *C. barbata*, the lemma primordium of the first floret arises (Fig. 16). Subsequently, the first floret primordium initiates (Fig. 17). The lemma of the second floret initiates alternately (Fig. 18). Simultaneously, the first floret primordium differentiates. The palea primordium initiates first (Fig. 19). Three stamen primordia arise after the formation of the palea (Fig. 20). Two of them are initiated on the lateral flanks of the primordium and one, abaxially (Fig. 21). Following the initiation of lemma of the third floret (Fig. 22), the gynoecial primordium of the first floret initiates and develops a gynoecial ridge surrounding the ovule primordium (Fig. 23). The lemma of the fourth floret initiates (Fig. 24). After that, the two lodicules of the first floret initiate in a whorl outside the stamen primordia (Fig. 25), and at the same time, the stamen primordia of the first floret expand to form thecae. Later, the filaments of each stamen gradually elongate, the style branches, and stigma develop. In *C. barbata*, the fourth floret primordium is reduced to a lemma vestigium without an awn. Therefore, there are three protruding awns on every spikelet at the end of anthesis (Figs. 1, 24). In *C. virgata*, only the second

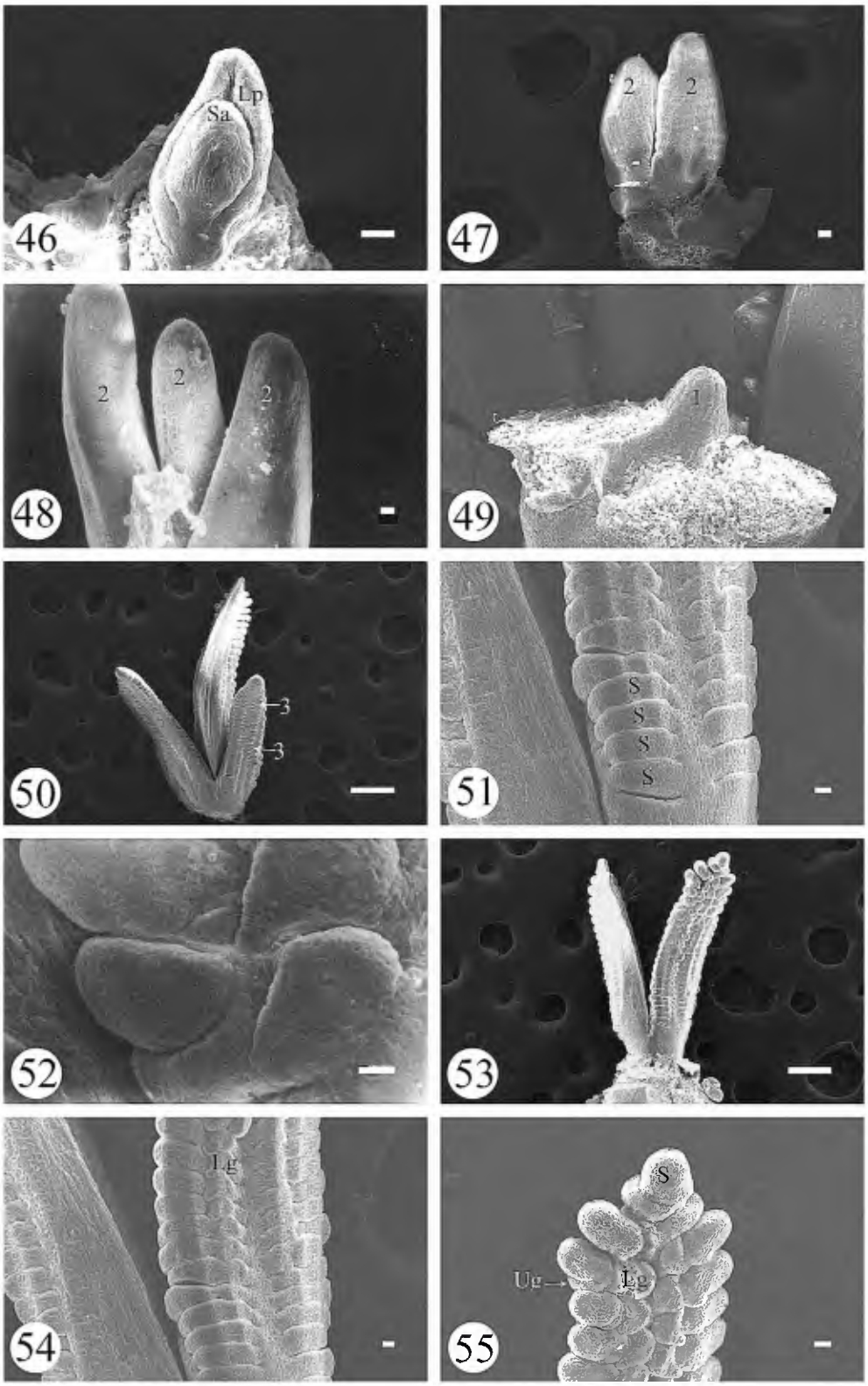

Figs. 46–55. *Eleusine indica* SEM micrographs. **46.** Vegetative shoot apex. **47.** Initiation of 2°-axis primordia, the 1° axis covered by two 2°-axis primordia. **48.** Elongation of 2°-axis primordia. **49.** Arrested 1° axis, 2°-axis primordia of semiverticillate arrangement removed. **50.** Initiation of peroblate 3°-axis primordia in basipetal succession. **51.** Proximal spikelet primordia of the 2° axis. **52.** Distal spikelet primordia of the 2° axis. **53.** Differentiation of spikelet primordia in basipetal succession. **54.** Initiation of lower glume. **55.** Initiation of upper glume and a spikelet primordium in 2°-axis apex. Scale bars = 10 μm in Figs. 46–49, 51, 52, 54, 55; 100 μm in Figs. 50, 53. See Figs. 8–17 for abbreviations.

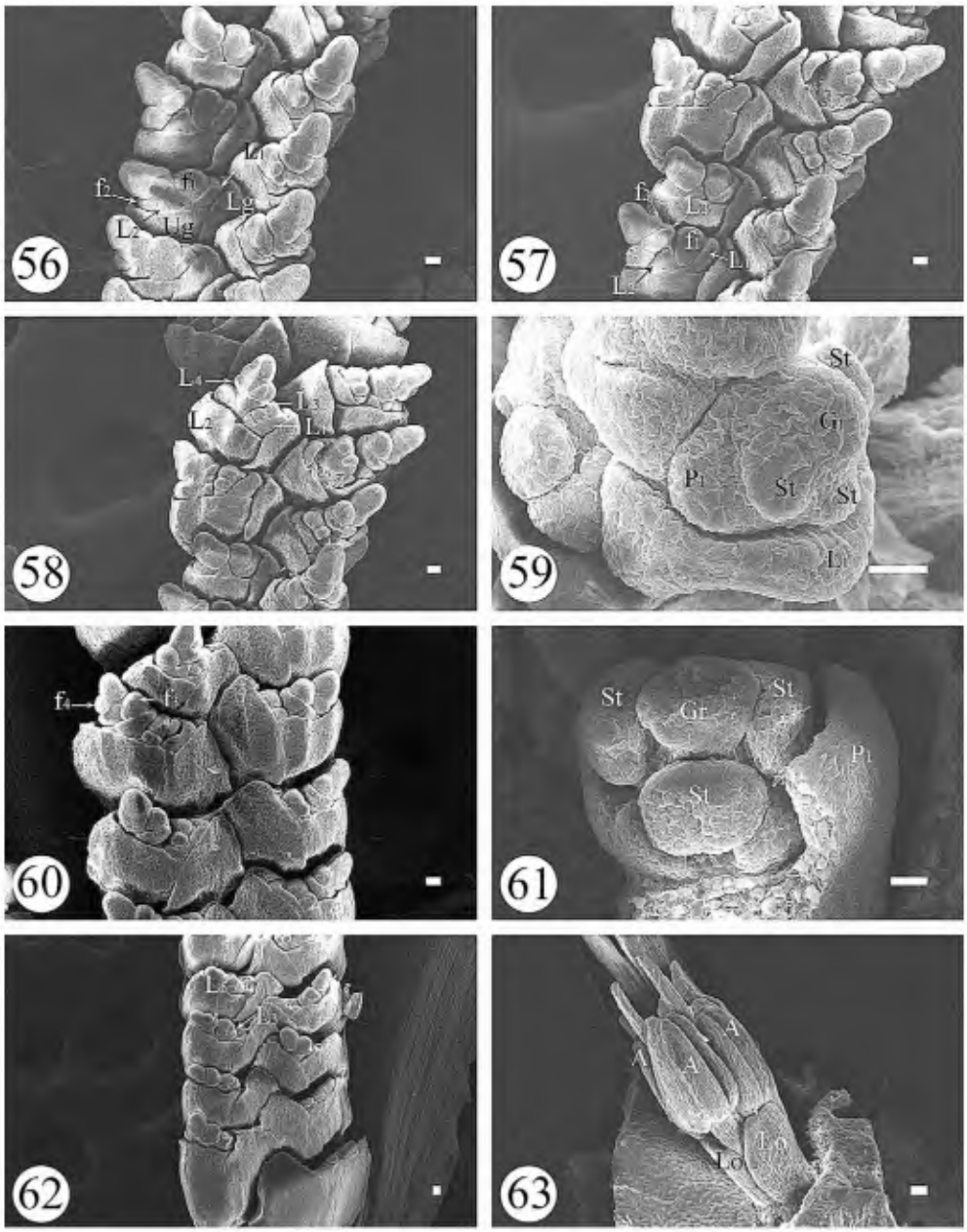

Figs. 56–63. *Eleusine indica* SEM micrographs. **56.** Initiation of first lemma, first floret primordium, second lemma and second floret primordium. **57.** Initiation of third lemma and third floret primordium. **58.** Initiation of fourth lemma. **59.** The first floret of left spikelet in Fig. 58, initiation of palea, stamen, and gynoecium. **60.** Initiation of fourth floret primordium, second floret primordium covered by upper glume. **61.** The first floret of left spikelet in Fig. 60, initiation of gynoecial ridge. **62.** Initiation of fifth lemma, second lemma and fourth lemma covered by upper glume. **63.** Differentiation of lodicules and anther of first floret. Scale bar = 10 μm. See Figs. 8–17 for abbreviations.

floret develops, with the lemma forming an awn. Therefore, there are two protruding awns on every spikelet at the end of anthesis (Figs. 2, 26). Finally, the 2° axis of both species ends in a blind extension (Fig. 27).

Cynodon—Inflorescence development of *Cynodon* starts with the formation of a suboblate 1°-axis primordium (Fig. 28). Elongation of the 1°-axis primordium stops (Fig. 29) after initiation of three to six 2°-axis primordia in *C. dactylon* and five to nine 2°-axis primordia in *C. arcuatus*. These 2°-axis primordia are verticillate and surround the arrested 1° axis (Figs. 30, 31). When these 2°-axis primordia elongate to nearly 325 μm, the oblate 3°-axis primordia initiate amphipetally on the 2° axis (Fig. 32). The proximal spikelet primordium is longer than the distal one (Fig. 34) (Table 1).

Spikelet differentiation on 2° axes of *C. dactylon* and *C. arcuatus* is amphipetal (Fig. 35) and starts with the formation of two alternate concave glume primordia (Fig. 36) on the abaxial surface of 2° axis. In addition, the 2° axis ends in an undifferentiated spikelet primordium (Fig. 37). The initiation of

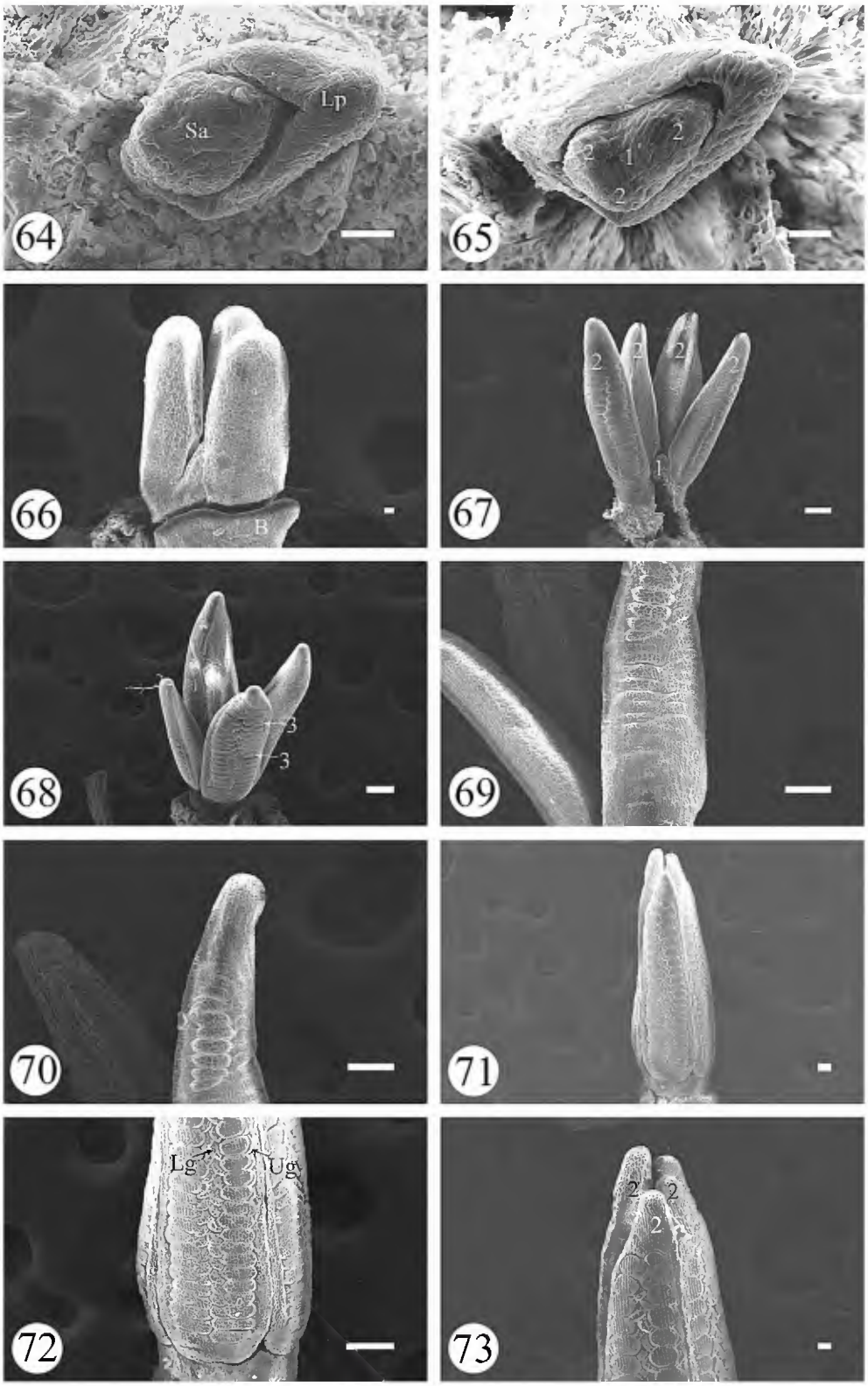

Figs. 64–73. *Dactyloctenium aegyptium* SEM micrographs. **64.** Vegetative shoot apex. **65.** Elongation of the 1°-axis primordium and initiation of 2°-axis primordia, viewed from above. **66.** Elongation of 2°-axis primordia. **67.** Semiverticillate arrangement of 2°-axis primordia surrounding the arrested 1° axis. **68.** Initiation of peroblate 3°-axis primordia in basipetal succession. **69.** Proximal spikelet primordia of the 2° axis. **70.** Distal spikelet primordia of the 2° axis. **71.** Differentiation of spikelet primordia in amphipetal succession. **72.** Initiation of lower and upper glumes. **73.** A microtip in 2°-axis apex. Scale bars = 10 μm in Figs. 64–66, 71, 73; 100 μm in Figs. 67–70, 72. See Figs. 8–17 for abbreviations.

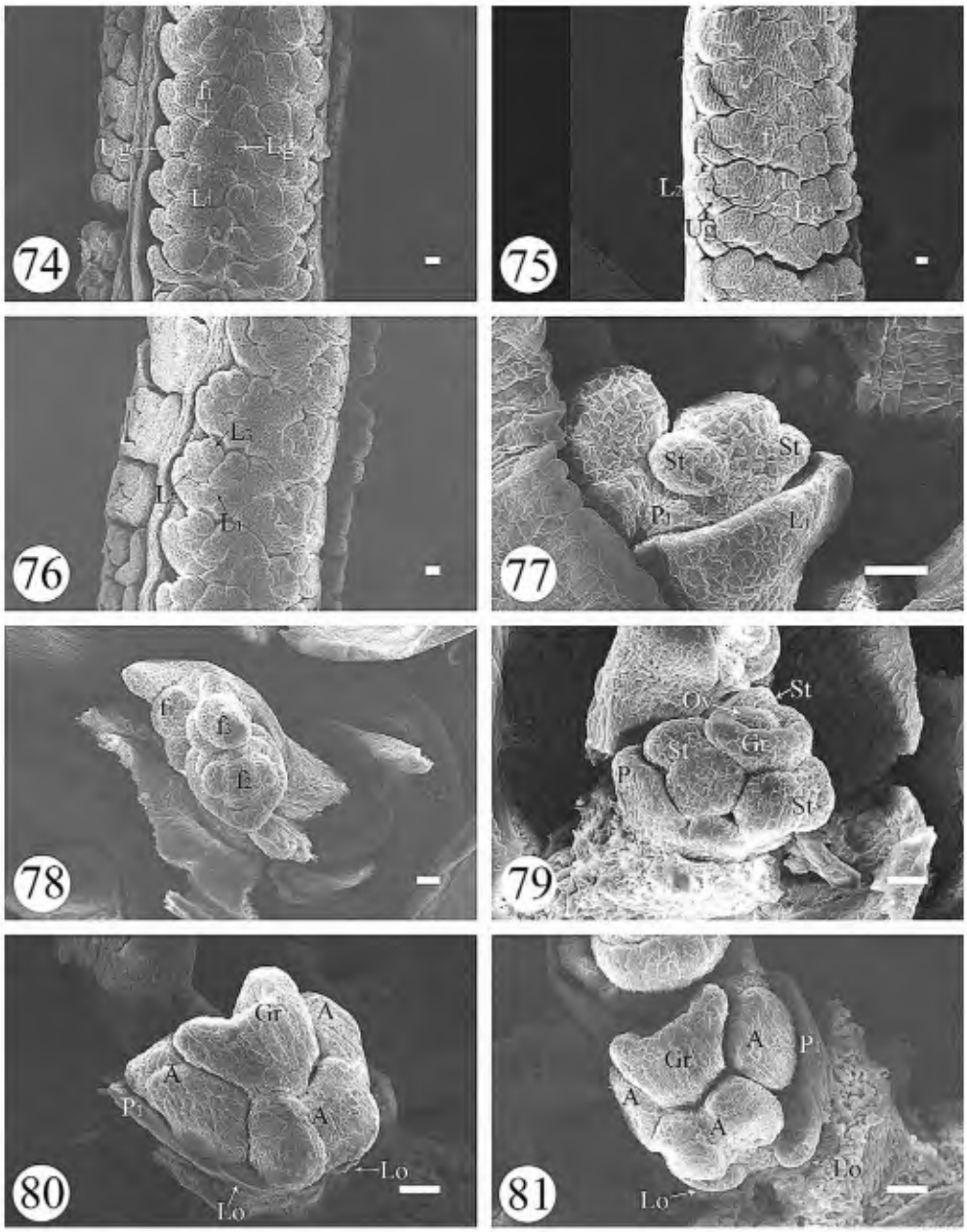

Figs. 74–81. *Dactyloctenium aegyptium* SEM micrographs. **74.** Initiation of first lemma and first floret primordium. **75.** Initiation of second lemma and second floret primordium. **76.** Initiation of third lemma. **77.** The first floret of left spikelet in Fig. 76, initiation of palea and stamen. **78.** Initiation of third floret primordium. **79.** The first floret of left spikelet in Fig. 78, initiation of gynoecial ridge of first floret. **80.** Differentiation of lodicules and anther of first floret. **81.** Formation of lodicules and elongation of filaments, viewed from above. Scale bar = 10 μm. See Figs. 8–17 for abbreviations.

florets along the spikelet axis is acropetal (Figs. 38–41). While the spikelet axis elongates, the lemma primordium of the first floret arises (Fig. 38). Almost simultaneously, the first floret primordium initiates (Fig. 39), and the lemma of second floret initiates alternately (Fig. 40). The second floret primordium then initiates (Fig. 41), and the remaining part of spikelet meristem develops into a degenerative floret. The palea primordium of the first floret initiates first (Fig. 42), and simultaneously three stamen primordia of first floret arise. Sequentially, the gynoecial primordium of the first floret initiates from the remaining part of floret primordium (Fig. 43) and develops a gynoecial ridge surrounding the ovule primordium. At the same time, stamen primordia of the first floret expand to form thecae. After that, the two lodicules of the first floret initiate in a whorl outside the thecae (Fig. 44). Later, stamen filaments gradually elongate, and style branches and stigma develop. By anthesis, the floral organs of every spikelet are completely enveloped by glumes (Fig. 3). Finally, the 2° axis ends in a degenerative spikelet (Fig. 45).

Eleusine—Inflorescence development of *Eleusine* starts with the formation of problate 1°-axis primordium (Fig. 46).

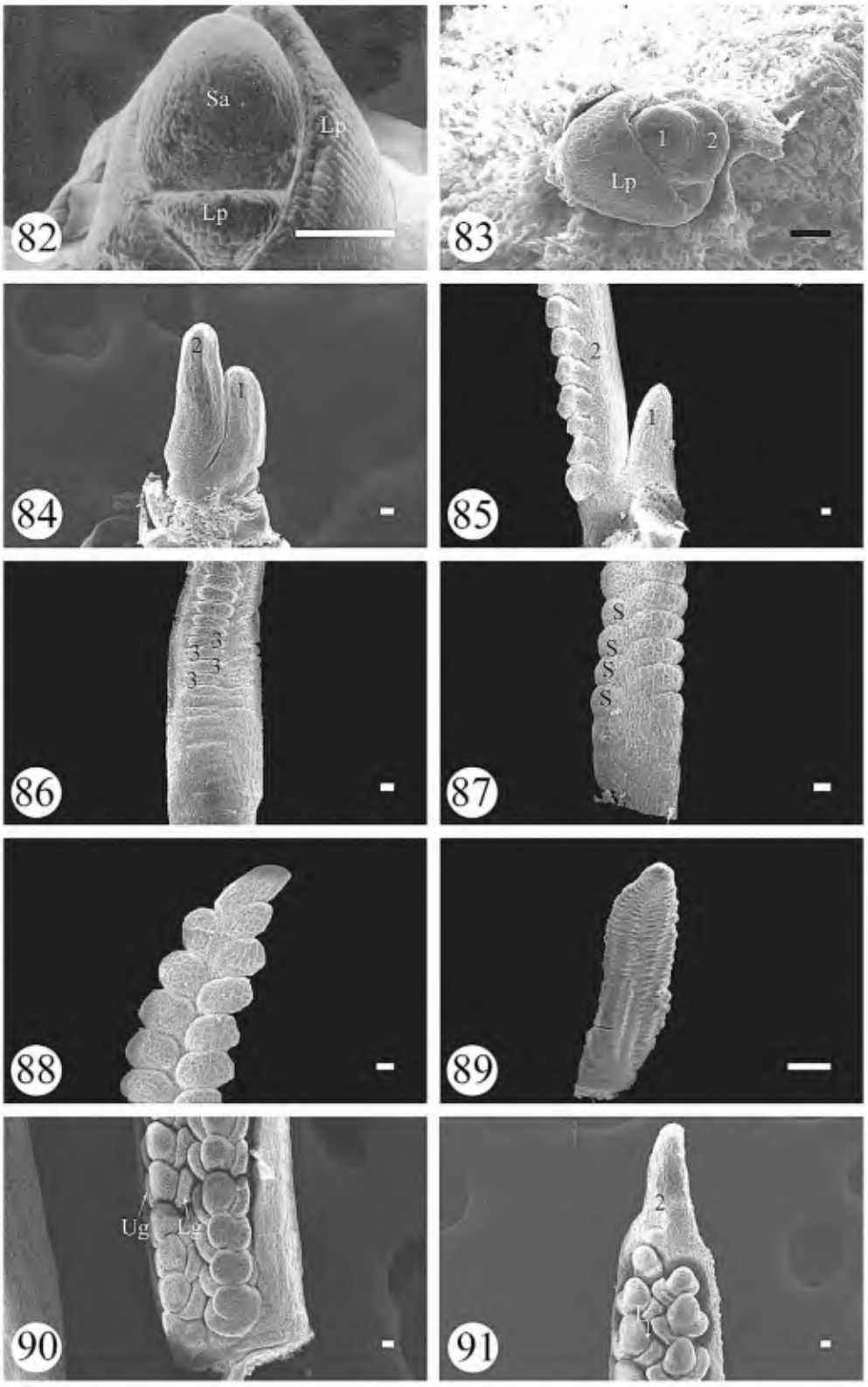

Figs. 82–91. *Microchloa indica* SEM micrographs. **82.** Vegetative shoot apex. **83.** Elongation of the 1°-axis primordium and initiation of the 2°-axis primordium, viewed from above. **84.** Elongation of both 1°-axis primordium and the 2°-axis primordium. **85.** Unilateral arrangement of the 2° axis and arrested 1° axis. **86.** Initiation of peroblate 3°-axis primordia in basipetal succession. **87.** Proximal spikelet primordia of the 2° axis. **88.** Distal spikelet primordia of the 2° axis. **89.** Differentiation of spikelet primordia in basipetal succession. **90.** Initiation of glumes and first lemma. **91.** A microtip in 2°-axis apex. Scale bar = 10 μm. See Figs. 8–17 for abbreviations.

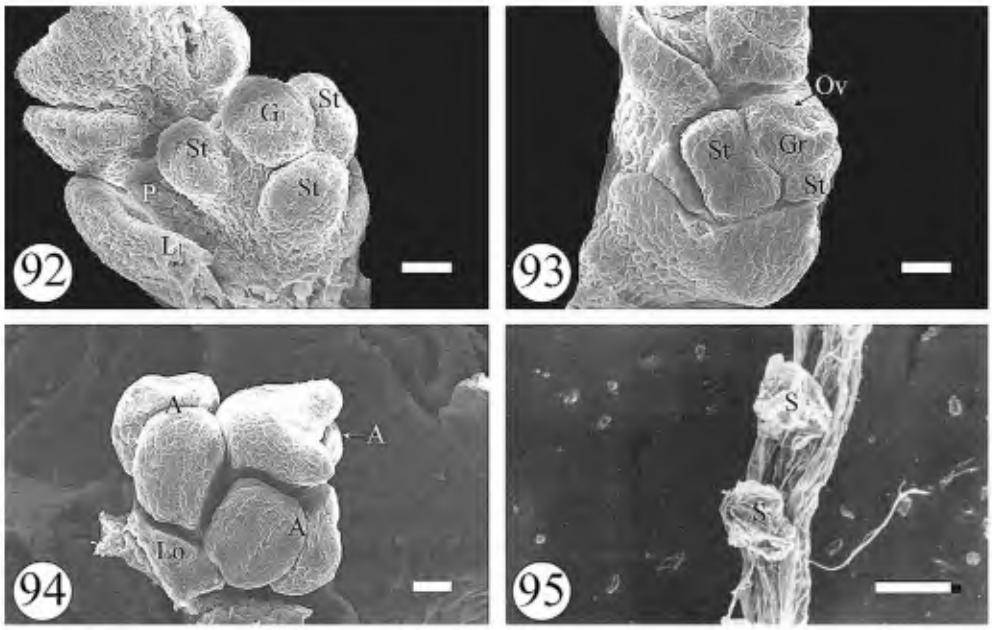

Figs. 92–95. *Microchloa indica* SEM micrographs. **92.** First floret of left spikelet in Fig. 91, initiation of palea and stamen. **93.** Initiation of gynoecial ridge. **94.** Differentiation of lodicules and anther. **95.** Distal degenerative spikelets covered by glumes. Scale bar = 10 μm. See Figs. 8–17 for abbreviations.

Elongation stops (Fig. 47) after the initiation of two to seven 2°-axis primordia in *E. indica* and seven to nine 2°-axis primordia in *E. coracana*. These 2°-axis primordia are semiverticillate and surround the arrested 1° axis (Figs. 48, 49). When these 2°-axis primordia elongate to nearly 646 μm, the peroblate 3°-axis primordia initiate basipetally on the 2° axis (Fig. 50). The proximal spikelet primordium (Fig. 51) is smaller than the distal one (Fig. 52) (Table 1).

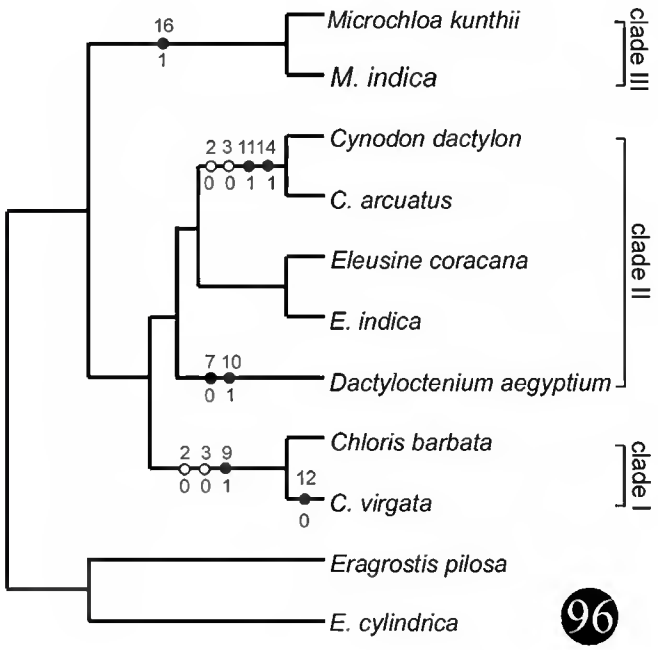

Fig. 96. Developmental characters mapped onto the parsimonious molecular tree using WinClada (Nixon, 2002). Numbers above branches are developmental characters; numbers below branches are character states; black circles represent nonhomoplastic synapomorphies; white circles represent homoplastic synapomorphies.

Spikelet differentiation on the 2° axis of *E. indica* is basipetal (Fig. 53) and starts with the formation of two keeled, concave glume primordia (Fig. 54) on the abaxial surface of 2° axis. In addition, the 2° axis ends in a differentiated spikelet primordium (Fig. 55). The initiation of florets along the spikelet axis of *E. indica* and *E. coracana* is acropetal (Figs. 56–58, 60). While the spikelet axis elongates, the lemma primordium of first floret arises, and almost simultaneously, the first floret primordium initiates (Fig. 56). The lemma of the second floret initiates alternately, and the second floret primordium then initiates (Fig. 56). The lemma of third floret initiates alternately, and the third floret primordium initiates (Fig. 57). Then the first floret primordium differentiates and the palea primordium initiates. Three stamen primordia arise after the formation of palea following the initiation of lemma of the fourth floret (Fig. 58). Then, the gynoecial primordium of first floret initiates from the remaining part of the floret primordium (Fig. 59). Accompanying the formation of the fourth floret primordium (Fig. 60), a gynoecial ridge forms surrounding the ovule primordium (Fig. 61). The lemma of fifth floret initiates (Fig. 62), and the two lodicules of the first floret subsequently initiate in a whorl outside the stamen primordia (Fig. 63); at the same time, stamen primordia of the first floret expand to form thecae. Later, the filaments of the stamens gradually elongate, and style branches develop. By anthesis, the floral organs of each spikelet are completely enveloped by the glumes. Finally, the 2° axis ends in a perfect spikelet in both species of *Eleusine* (Fig. 4).

Dactyloctenium—Inflorescence development of *Dactyloctenium aegyptium* starts with the formation of a problate 1°-axis primordium (Fig. 64). Elongation stops after the initiation of two to six 2°-axis primordia (Fig. 65). These 2°-axis primordia are semiverticillate and surround the arrested 1° axis (Figs. 66,

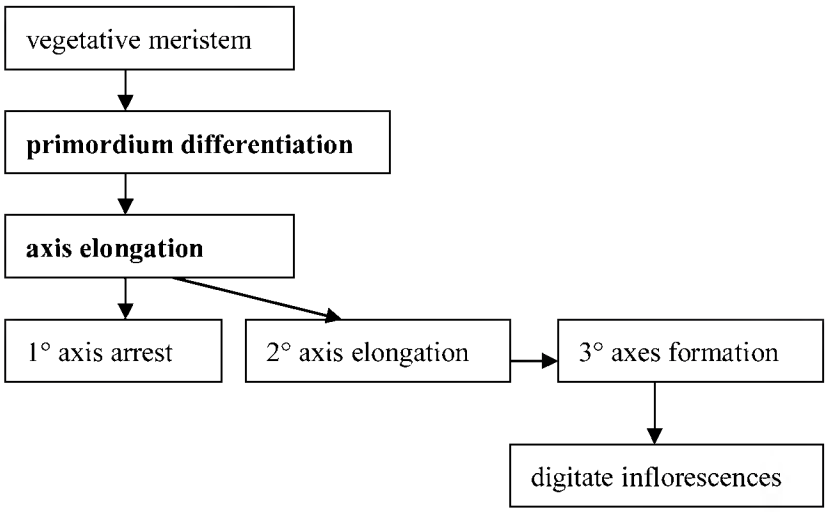

Fig. 97. Schematic diagrams of digitate inflorescence formation. Arrows indicate genetic pathways. Bold characters indicate the critical developmental changes.

67). When these 2°-axis primordia elongate to nearly 666 μm, the peroblate 3°-axis primordia initiate basipetally on the 2° axis (Fig. 68). The proximal spikelet primordium (Fig. 69) is longer than the distal one (Fig. 70).

Spikelet differentiation on the 2° axis of *Dactyloctenium aegyptium* is amphipetal (Fig. 71) and starts with the formation of concave glume primordia (Fig. 72) on the abaxial surface of 2° axis. In addition, the 2° axis ends in a microtip (Fig. 73). The initiation of florets along the spikelet axis of *D. aegyptium* is acropetal (Figs. 74–76), and while the spikelet axis elongates, the lemma primordium of the first floret arises. Almost simultaneously, the first floret primordium initiates (Fig. 74), and the lemma of the second floret initiates alternately; the second floret primordium then initiates (Fig. 75). The lemma of the third floret initiates alternately (Fig. 76), and then the first floret primordium differentiates. The palea primordium initiates first, and three stamen primordia arise after the formation of palea (Fig. 77). Following the initiation of the third floret primordium (Fig. 78), the gynoecial primordium of the first floret differentiates. Accompanying the differentiation of second floret, the gynoecial ridge develops and surrounds the ovule primordium (Fig. 79). Subsequently, the two lodicules of the first floret initiate in a whorl outside the stamen primordia (Fig. 80), and at the same time, stamen primordia of first floret expand to form thecae. Later, stamen filaments elongate when the two lodicules (Fig. 81) and style branches develop. By anthesis, the floral organs of each spikelet are completely enveloped by glumes, and finally, the 2° axis ends in a microtip (Fig. 5).

Microchloa—Inflorescence development of *Microchloa* starts with the formation of a prolate 1°-axis primordium (Fig. 82). Elongation stops after the initiation of one 2°-axis primordium (Fig. 83). The 2°-axis primordium is located unilateral to the arrested 1° axis (Figs. 84, 85). When the 2°-axis primordium elongates to nearly 320 μm, the peroblate 3°-axis primordia initiate basipetally on the 2° axis (Fig. 86). The proximal spikelet primordium (Fig. 87) is smaller than the distal one (Fig. 88) in both species of *Microchloa* (Table 1).

Spikelet differentiation on the 2° axis of *Microchloa* is basipetal (Fig. 89) and starts with the formation of two concave glume primordia (Fig. 90) on the abaxial surface of 2° axis. In addition, the 2° axis ends in a microtip (Fig. 91), while the lemma primordium of first floret arises (Fig. 91). Almost simultaneously, the first floret primordium initiates. The palea primordium initiates first, and three stamen primordia (E = 20 μm) arise sequentially (Fig. 92). The gynoecial primordium of the first floret initiates and develops a gynoecial ridge that surrounds the ovule primordium (Fig. 93). Subsequently, two lodicules of the first floret initiate in a whorl outside the stamen primordia (Fig. 94). At the same time, the stamen primordia of the first floret expand to form thecae. The style branches develop later. By anthesis, the distal spikelets are incompletely developed and enveloped by glumes (Fig. 95), and finally, the 2° axis ends in a microtip.

In all species examined, elongation of the culm below the inflorescence peduncle occurred late in development, i.e., after the formation of glumes until before maturation of the caryopsis. Culm length varies between 1.5–9.0 cm for all species (Table 1).

Distribution of developmental characters on a molecular tree—Three characters were uninformative when mapped onto the cladgram (Fig. 96, Table 1). Of the remaining characters that were informative, two appear as homoplastic synapomorphies (characters 2 [Dt of 1°-axis primordium] and 3 [100·Dp/Dt of 1°-axis primordium]), and six characters appear as nonhomoplastic synapomorphies (characters 7 [arrangement of 2°-axis primordia], 9 [length of 2°-axis at the moment of 3°-axis initiation], 10 [end of 2° axis], 11 [peduncle length], 14 [P of distal spikelet primordium], and 16 [initiation succession of spikelets on 2° axis]).

DISCUSSION

Phylogeny—Ingroup taxa were chosen to cover the major morphological groups in the finger millet clade (Hilu and Alice, 2001; Liu et al., 2005a). Although these results need to be confirmed with data from more taxa, it is interesting to

explore the implications of the typology discovered. With two *Eragrostis* species used as outgroups (Hilu and Alice, 2001), *Microchloa*, *Cynodon*, *Eleusine*, *Dactyloctenium*, and *Chloris* formed a monophyletic group in the most parsimonious tree. Within this finger millet clade, three major clades were recovered, with clades I and III consisting of species of *Chloris* and *Microchloa*, respectively, and clade II including species of *Cynodon*, *Eleusine*, and *Dactyloctenium*. Clade III was found to be sister to clade I/II.

Our results suggest that *Eleusine* and *Dactyloctenium* should be included in the subtribe Choridinae. The monophyletic group composed by clade I/II has high bootstrap support (100%) and contains two well-supported clades. Clade I consists of plants with one fertile floret per spikelet, and clade II consists of plants with two to many fertile florets per spikelet. Therefore, Clayton and Renvoize (1986) included *Chloris*, *Cynodon*, and *Microchloa* in the Chloridinae and *Eleusine* and *Dactyloctenium* in the Eleusininae. Peterson et al. (2001) included *Eleusine* and *Dactyloctenium* in the Eleusininae. Hilu and Alice (2001) grouped *Eleusine* and *Dactyloctenium* in a weakly supported clade with phylogenetic affinities with other genera in the Chloridinae. The relationship between clades I and II in this study reflects morphological similarities in developmental characters such as two to nine 2° axes surrounding the 1° axis (character 6), semiverticillate or verticillate arrangement of the 2°-axis primordia (character 7), laterally compressed spikelets (character 17), and 2–5 florets per spikelet (character 19). Because the two subtribes Eleusininae and Chloridinae do not seem to be natural taxonomic units, especially for those taxa undergoing rapid speciation, these groups should be reclassified after more species have been sampled to gain a better understanding of their evolutionary relationships (Peterson et al., 1997; Jacobs and Everett, 2000).

Clade III, which comprises two species of *Microchloa*, has strong bootstrap support (99%). Our analysis confirms the sister relationship between *Microchloa* and *Chloris* allies because these genera form a strongly supported finger clade (99%). The distinct developmental characters of clade III are the single 2°-axis primordium (character 6) and the unilateral arrangement of the 2° axis (character 7). Because *Microchloa* is one of the early derived lineages, we hypothesize that digitate inflorescences with a single 2° axis arose relatively early in the evolutionary history of finger millet clade.

Combined analysis—The overall picture of development is one of early similarity followed by later diversification. Developmental characters were optimized onto one parsimonious cladogram and were mostly congruent with the molecular phylogeny. The combined analysis had an identical topology with the molecular tree (Fig. 7). Clade I/II as a whole and clade II are not defined by any developmental characters, but clade III is defined by the basipetal succession of spikelet initiation on the 2° axis (character 16). *Dactyloctenium* (clade II) is defined by two characters: semiverticillate arrangement of the 2°-axis primordia (character 7) and a microtip in the end of the 2° axis (character 10).

The equatorial axis diameter of the 1°-axis primordium (character 2) and 100·Dp/Dt of 1°-axis primordium (character 3) originated twice, once within *Cynodon* (clade II) and once within *Chloris* (clade I). The parallel derivation of homoplastic synapomorphies suggests that these character states (characters 2 and 3) in *Cynodon* may not be homologous with the structures in *Chloris*.

In most cases, temporal variation in developmental characters would not have been detected by investigating mature morphology. For example, *D. aegyptium* (Fig. 5) differs from *C. virgata* (Fig. 2) in having a lax digitate inflorescence (Figs. 2, 5). Initiation of the 2°-axis promordia occured early in both genera, but further spread of the axes did not occur in *C. virgata*, resulting in a contracted inflorescence at maturity. In contrast, the spread of 2° axes occurred late in the development of *D. aegyptium*, leading to a distinctly spreading inflorescence.

In addition to traditional morphological studies, developmental analysis can also provide novel explanations for interpreting differences among genera. In the monophyletic finger millet clade, the end of the 2° axis has been used as a diagnostic taxonomic character (Chen, 1990). In species of *Microchloa*, the 2° axis terminates with a microtip, while in others, such as species of *Cynodon*, the 2° axis terminates with a spikelet. Early in their development, however, all species have a similar terminal morphology of the 2° axis. Differences appear at maturity because spikelets are initiated basipetally along the 2° axis in species of *Microchloa* with the microtip remaining undifferentiated in its initial developmental stage, while in *Cynodon* spikelets are initiated amphipetally along the 2° axis, with a spikelet primordium at the end of the 2° axis late in development. Therefore, the "character" of the end of the 2° axis is composed of another developmental character, i.e., initiation of a spikelet on a 2° axis. In contrast, in species of *Cynodon*, the end of the 2° axis is determined later in development and thus is truly nonhomologous to the end of 2° axis in species of *Microchloa*.

The role of developmental variation in inflorescence formation in the finger millet clade can be diagrammed using the simple model in Fig. 97. Changes involving primordium differentiation that result from activity of the apical meristem for all orders of axes occur very early. Changes involving axis elongation, including the arrest of the 1° axis, the elongation of 2° axes, and the formation of 3° axes (i.e., spikelets), occur much later. For different grass groups, axis elongation plays a critical role in the external appearance of the inflorescence. For example, the arrest of the 1° axis in the finger millet clade determines that the main axis terminates in a remnant and forms a digitate inflorescence, while in the bristle clade (Doust and Kellogg, 2002), the 1° axis continually develops to maturity and forms a paniculate inflorescence. Therefore, the remarkable discrimination of development of the same character suggests that the various developmental characters may be under different genetic control (Kellogg, 2004).

Our observations confirm that there is no distinct morphological variation among several long paraclades in the finger millet clade. This supports the theory that several long paraclades are actually 2° axes circling the truncated main axis (Cámara-Hernández and Rua, 1991; Liu et al., 2005a). Studies of gene expression involved in axis elongation are needed to elucidate inflorescence diversification in the finger millet clade. The external appearance of maize inflorescence is regulated by three *RAMOSA* genes, i.e., *RA1*, *RA2*, and *RA3* (Vollbrecht et al., 2005; Bortiri et al., 2006; Satoh-Nagasawa et al., 2006). The *RA2* is critical for shaping the initial steps of inflorescence formation in the grass family because *RA2* controls the expression of other genes and regulates the activity of the 2°-axis primordia. The *RA2* also controls the expression

pattern and is conserved in other grasses including rice, barley, and sorghum (Bortiri et al., 2006). Given this current knowledge, any of the three genes could be involved in the activity of the 2°-axis primordia in the finger millet clade. Accordingly, analysis of the *RA2* gene expression and the interplay between three *RAMOSA* genes in the finger millet clade may elucidate the molecular mechanism underlying the branching pattern of digitate inflorescences.

LITERATURE CITED

BARKER, F. K., AND F. M. LUTZONI. 2002. The utility of the incongruence length difference test. *Systematic Biology* 51: 625–637.

BORTIRI, E., G. CHUCK, E. VOLLBRECHT, T. ROCHEFORD, R. MARTIENSSEN, AND S. HAKE. 2006. *RAMOSA2* encodes a LATERAL ORGAN BOUNDARY domain protein that determines the fate of stem cells in branch meristems of maize. *Plant Cell* 18: 574–585.

CÁMARA-HERNÁNDEZ, J., AND G. H. RUA. 1991. The synflorescence of Poaceae. *Beiträge zur Biologie der Pflanzen* 66: 297–311.

CHEN, S. L. 1990. Gramineae (4)—subfamily Eragrostoideae Pilger. *In* S. L. Chen [ed.], Flora reipublicae popularis sinicae, vol. 10, 1–131. Science Press, Beijing, China.

CLAYTON, W. D., AND S. A. RENVOIZE. 1986. Genera graminum. Kew Bulletin Additional Series XIII. Her Majesty's Stationery Office, London, UK. 389.

DOUST, A. N., AND E. A. KELLOGG. 2002. Inflorescence diversification in the panicoid "bristle grass" clade (Paniceae, Poaceae): evidence from molecular phylogenies and developmental morphology. *American Journal of Botany* 89: 1203–1222.

DOYLE, J. J., AND J. L. DOYLE. 1987. A rapid DNA isolation procedure for small quantities of fresh tissues. *Phytochemical Bulletin* 19: 11–15.

ERDTMAN, G. 1952. Pollen morphology and plant taxonomy—angiosperms. Almqvist and Wilksell, Stockholm, Sweden. 466.

FARRIS, J. S., M. KÄLLERSJÖ, A. G. KLUGE, AND C. BULT. 1995. Testing significance of incongruence. *Cladistics* 10: 315–319.

FARRIS, J. S., A. G. KLUGE, AND M. J. ECKARDT. 1970. A numerical approach to phylogenetic systematics. *Systematic Zoology* 19: 172–191.

FELSENSTEIN, J. 1981. Evolutionary trees from DNA sequences: a maximum likelihood approach. *Journal of Molecular Evolution* 17: 368–376.

FELSENSTEIN, J. 1985. Confidence limits of phylogenies: an approach using the bootstrap. *Evolution* 39: 783–791.

FITCH, W. 1971. Toward defining the course of evolution: minimum change for a specific tree typology. *Systematic Zoology* 20: 406–416.

GOLOBOFF, P. A. 1993. NONA version 2.0. Computer program published by the author, Tucumán, Argentina (available at http://www.cladistics.com).

HILU, K. W., AND L. A. ALICE. 2001. A phylogeny of Chloridoideae (Poaceae) based on *mat*K sequences. *Systematic Botany* 26: 386–405.

HIPP, A. L., J. C. HALL, AND K. J. SYTSMA. 2004. Congruence versus phylogenetic accuracy: revisiting the incongruence length difference test. *Systematic Biology* 53: 81–89.

HUFFORD, L. 2003. Homology and developmental transformation: models for the origins of the staminodes of Loasaceae subfamily Loasoideae. *International Journal of Plant Sciences* 164 (5 Supplement): S409–S439.

JACOBS, S. W. L., AND J. EVERETT. 2000. Grasses: systematics and evolution. CSIRO, Collingwood, Victoria, Australia.

KELLOGG, E. A. 2004. Evolution of developmental traits. *Current Opinion in Plant Biology* 7: 92–98.

KENG, Y. L. 1959. Flora illustralis plantarum primarum sinicarum Gramineae. Science Press, Beijing, China.

LIU, Q., N. X. ZHAO, AND G. HAO. 2005a. Inflorescence structures and evolution in subfamily Chloridoideae (Gramineae). *Plant Systematics and Evolution* 251: 183–198.

LIU, Q., N. X. ZHAO, AND G. HAO. 2005b. Phylogenetic relationships of the Chloridoideae (Gramineae): a cladistic analysis. *Journal of Tropical and Subtropical Botany* 13: 432–442.

MADDSION, D. R., AND W. P. MADDSION. 2000. MacClade, version 4.0. Sinauer, Sunderland, Massachusetts, USA.

NIKLAS, K. J. 1987. Pollen capture and wind-induced movement of compact and diffuse grass panicles: implications for pollination efficiency. *American Journal of Botany* 74: 74–89.

NIXON, K. C. 2002. WinClada, version 1.00.08. Computer program published by the author, Ithaca, New York, USA (available at http://www.cladistics.com).

OXELMAN, B., M. LIDÉN, AND D. BERGLUND. 1997. Chloroplast *rps*16 intron phylogeny of the tribe Sileneae (Caryophyllaceae). *Plant Systematics and Evolution* 206: 393–410.

PETERSON, P. M., R. J. SORENG, G. DAVIDSE, T. S. FILGUEIRAS, F. O. ZULOAGA, AND E. J. JUDZIEWICZ. 2001. Catalogue of New World grasses (Poaceae). II. Subfamily Chloridoideae. *Contributions from the United States National Herbarium* 41: 1–255.

PETERSON, P. M., R. D. WEBSTER, AND J. VALDES-REYNA. 1997. Genera of New World Eragrostideae (Poaceae: Chloridoideae). *Smithsonian Contributions to Botany* 87: 1–50.

POE, S., AND J. J. WIENS. 2000. Characters selection and the methodology of morphological phylogenetics. *In* J. J. Wiens [ed.], Phylogenetic analysis of morphological data, 20–36. Smithsonian Institution Press, Washington, D.C., USA.

POSADA, D., AND K. A. CRANDALL. 1998. MODELTEST: testing the model of DNA substitution. *Bioinformatics* 14: 817–818.

ROODT, R., AND J. J. SPIES. 2003. Chromosome studies in the grass subfamily Chloridoideae. I. Basic chromosome numbers. *Taxon* 53: 557–566.

SATOH-NAGASAWA, N., N. NAGASAWA, S. MALCOMBER, H. SAKAI, AND D. JACKSON. 2006. A trehalosa metabolic enzyme controls inflorescence architecture in maize. *Nature* 441: 227–230.

SHAW, J., AND R. L. SMALL. 2004. Addressing the "hardest puzzle in American pomology": phylogeny of *Prunus* sect. *Prunocerasus* (Rosaceae) based on seven noncoding chloroplast DNA regions. *American Journal of Botany* 91: 985–996.

STEVENS, P. F. 1991. Character states, morphological variation, and phylogenetic analysis: a review. *Systematic Botany* 16: 553–583.

STUESSY, T. F. 2003. Morphological data in plant systematics. *In* T. F. Stuessy, V. Mayer, and E. Hörandl [eds.], Deep morphology: toward a renaissance of morphology in plant systematics, 299–315. Gantner, Koeltz, Königstein, Germany.

SWOFFORD, D. L. 2002. PAUP*: phylogenetic analysis using parsimony (*and other methods), version 4.0b10. Sinauer, Sunderland, Massachusetts, USA.

TABERLET, P., L. GIELLY, G. PAUTOU, AND J. BOUVET. 1991. Universal primers for amplification of three non-coding regions of choroplast DNA. *Plant Molecular Biology* 17: 1105–1109.

THOMPSON, J. D., T. J. GIBSON, F. PLEWNIAK, F. EANMOUGIN, AND D. G. HIGGINS. 1997. The ClustalX windows interface: flexible strategies for multiple sequence alignment aided by quality analysis tools. *Nucleic Acids Research* 25: 4876–4882.

VAN DEN BORRE, A., AND L. WATSON. 1997. On the classification of the Chloridoideae. *Australian Systematic Botany* 10: 491–531.

VEGETTI, A. C. 1986. Contribución al conocimiento de las inflorescencias en *Chloris* y *Cynodon* (Poaceae). *Kurtziana* 18: 109–120.

VOLLBRECHT, E., P. S. SPRINGER, L. GOH, E. S. BUCKLER, AND R. MARTIENSSEN. 2005. Architecture of floral branch systems in maize and related grasses. *Nature* 436: 1119–1126.

WIENS, J. J. 2001. Character analysis in morphological phylogenetics: problem and solutions. *Systematic Biology* 50: 689–699.

YODER, A. D., J. A. IRWIN, AND B. A. PAYSEUR. 2001. Failure of the ILD to determine data combinability for slow *Loris* phylogeny. *Systematic Biology* 50: 408–424.

Appendix 1. Voucher information and GenBank accession numbers for sequences for the *trnL* and *rps16* introns for the taxa used in this study. Voucher specimens are deposited in the following herbaria: IBSC = Herbarium of South China Botanical Garden, the Chinese Academy of Sciences; QL = Qing LIU.

Taxon—GenBank accessions: *trnL*, *rps16*; Source; *Voucher specimen.*

Chloris barbata Sw.—AY787812, DQ242043; Hainan, China; QL 05026, IBSC. ***C. virgata*** Sw.—AY787813, DQ242043; Yunnan, China; QL 02022, IBSC. ***Cynodon dactylon*** (L.) Pers.—AY787808, DQ242038; Guangdong, China; QL 04035, IBSC. ***C. arcuatus*** J. Presl et C. Presl—AY787807, DQ242039; Hainan, China; QL 02016, IBSC. ***Eleusine coracana*** (L.) Gaertn.—AJ489464[a], DQ242040; Anhui, China; QL 03020, IBSC. ***E. indica*** (L.) Gaertn.—AY787806, DQ242041; Yunnan, China; QL 02028, IBSC. ***Dactyloctenium aegyptium*** (L.) P.Beauv.—AY787809, DQ242042; Hainan, China; QL 05074, IBSC. ***Microchloa kunthii*** Desv.—AY787814, DQ242045; Yunnan, China; QL 02060, IBSC. ***M. indica*** (L. f.) P. Beauv.—AY787815, DQ242046; Hainan, China; QL 02012, IBSC. ***Eragrostis pilosa*** (L.) P. Beauv.—AY787810, AY136859[a]; Guangdong, China; QL 02091, IBSC. ***E. cylindrica*** (Roxb.) Nees—AY787811, DQ242047; Yunnan, China; QL 02060, IBSC.

[a]Archived GenBank sequences